Electrocatalysis

DOI: 10.1002/anie.201307475

Two-Dimensional Hybrid Nanosheets of Tungsten Disulfide and Reduced Graphene Oxide as Catalysts for Enhanced Hydrogen Evolution**

Jieun Yang, Damien Voiry, Seong Joon Ahn, Dongwoo Kang, Ah Young Kim, Manish Chhowalla, and Hyeon Suk Shin**

Monolayers of transition-metal dichlacogenides (TMDs) have been recently receiving interest for both fundamental and technological investigations. One key to the realization of the potential of TMDs is the synthesis of high-quality materials. One interesting TMD compound is WS_2 in which the electrical properties can be varied from metallic and semiconducting by tuning the crystal structure and the number of layers.[1] Conventionally mono- or few-layered WS_2 can be obtained by mechanical exfoliation or grown by chemical vapor deposition (CVD), using precursors such as $WOCl_4$ and $HS(CH_2)_2SH$.[1a,2] In addition, chemical methods for large-scale synthesis of layered WS_2 have been reported. For example, WS_2 nanosheets with lateral dimensions of 100 nm have been synthesized from one-dimensional (1D) $W_{18}O_{49}$ with assistance of surfactants through a rolling-out method.[3] Recently, a powder of WS_2 nanosheets was obtained by a two-step process that involves mixing WO_3 and S by ball milling and heating the mixture and S powder to 600 °C in Ar.[4] A solid-state reaction with tungstic acid and thiourea in N_2 atmosphere at 773 K has also produced layered WS_2.[5]

The hydrothermal reaction is known to be a facile method for large scale manufacturing of TMD nanosheets at relatively low temperature. The synthesis of MoS_2 sheets has been well studied using precursors such as sodium molybdate and thioacetamide or thiourea as the S source.[6] Although inorganic fullerene-like (IF) WS_2 nanoparticles, 1D nanotubes, or 1D rods have been obtained by the hydrothermal method,[7,8] synthesis of WS_2 sheets by the hydrothermal reaction has yet to be realized. The primary reason for this is due to the fact that the WO_x precursor required for the formation of WS_2 nanosheets does not occur in 2D form. Instead WO_x prefers to form 1D or zero-dimensional (0D) nanostructures. Thus sulfurization of the WO_x favors the formation of 0D fullerene-like or 1D nanotube/nanorod like WS_2 nanostructures. This is in contrast to MoS_2 nanosheets in which the MoO_3 precursor is a layered compound.[9,10] The absence of a facile WS_2 nanosheet synthesis method has also prevented the study of WS_2/graphene hybrid structures, despite their potentially useful applications. We therefore develop a hydrothermal method for synthesis of WS_2 nanosheets and then we integrate rGO nanosheets into the reactor to fabricate novel WS_2/rGO hybrids. We report detailed structural analyses of the synthesized products and investigate their potential catalysts for the hydrogen evolution reaction (HER). The primary uniqueness of our work is the synthesis of WS_2 and rGO/WS_2 nanosheets using a scalable hydrothermal method and their implementation as efficient catalysts for HER.

MoS_2 nanostructures are promising electrocatalysts for H_2 production.[11] The overpotential of MoS_2 catalysts is −200–−150 mV and Tafel slopes are in a range of 55–40 mV dec^{-1} (millivolts per decade).[11–13] Recent results have suggested that WS_2 nanosheets could be interesting as HER electrocatalysts. An overpotential of −60 mV and a Tafel slope of about 70 mV dec^{-1} have been measured for WS_2 sheets synthesized by the ball-milling method[4] while values of −150 mV and about 70 mV dec^{-1} have been obtained for WS_2 particles on carbon cloth.[12] Voiry et al. showed that both the overpotential (−100 mV) and Tafel slopes (60 mV dec^{-1}) can be lowered by used WS_2 nanosheet catalysts that contain a high concentration of the metallic 1T phase.[14]

Herein, we report the synthesis of WS_2 and WS_2/rGO nanosheets using an one-pot hydrothermal reaction process at low temperature. We show that WS_2 nanosheets are selectively fabricated using tungsten chloride and thioacetamide precursors. We also show that WS_2 nanosheets readily hybridize with rGO nanosheets when GO is added in the reaction vessel. This is one of the first reports on selective synthesis of WS_2 and WS_2/rGO hybrid nanosheets by the hydrothermal reaction. We further demonstrate that WS_2/rGO nanosheets exhibit good catalytic activity for hydrogen evolution. Based on impedance measurements, the better catalytic performance is attributed to enhanced charge trans-

[*] J. Yang,[+] S. J. Ahn, D. Kang, A. Y. Kim, Prof. H. S. Shin
Interdisciplinary School of Green Energy and
Low Dimensional Carbon Materials Center
Ulsan National Institute of Science and Technology(UNIST)
UNIST-gil 50, Ulsan 689-798 (Republic of Korea)
E-mail: shin@unist.ac.kr
D. Voiry,[+] Prof. M. Chhowalla
Materials Science and Engineering Department
Rutgers University
607 Taylor Road, Piscataway, NJ (USA)
E-mail: manish1@rci.rutgers.edu
[+] These authors contributed equally to this work.

[**] This work was supported by the Basic Science Research Program (2011-0013601) and a grant (grant number 2011-0031630) from the Center for Advanced Soft Electronics under the Global Frontier Research Program through the National Research Foundation funded by the Ministry of Science, ICT and Future Planning, Korea. We thank Prof. Sang Hoon Joo for helpful discussion.

Supporting information for this article is available on the WWW under http://dx.doi.org/10.1002/anie.201307475.

fer kinetics due to the intimate contact between the catalytic WS_2 nanosheets and the rGO support.

The hydrothermal synthesis of WS_2 is known to be sensitive to temperature. 1D WS_2 structures have been synthesized at 265 °C through WO_3 intermediates, whereas no WS_2 has been synthesized below 240 °C.[7] In a typical process, tungstate precursors such as Na_2WO_4 or $(NH_4)_{10}W_{12}O_{41}$ react with acid to condense WO_x nanoparticles or 1D nanostructures that are sulfurized to give WS_2.[7,8] The WO_x nanoparticles or 1D structures act as templates for the formation of WS_2. The conversion of WO_x to WS_2 is not fully explained yet. In this study, we employ WCl_6 as a precursor for W which has been used for vapor phase rection in CVD and not induced WO_x.[15,16] The hydrothermal method was carried out at 265 °C for 24 hrs using WCl_6, thioacetamide (TAA), and graphene oxide (GO) to produce WS_2/rGO hybrid sheets. (See Supporting Information for experimental details.) In the absence of GO, only WS_2 sheets are synthesized. During the hydrothermal reaction, WCl_6 and TAA produces WS_2 on GO sheets and GO is reduced to rGO. As-prepared WS_2/rGO hybrid sheets are then freeze-dried and annealed at 300 °C to improve the crystallinity of the nanosheets. The reaction process is supposed to be as shown in Scheme 1 and Equations (1) and (2).[16]

$$C_2H_5NS + 2\,H_2O \rightarrow H_2S + NH_3 + CH_3COOH \quad (1)$$

$$WCl_6 + 3\,H_2S \rightarrow WS_2 + 6\,HCl + S \quad (2)$$

Here, H_2S is released from TAA and reduce WCl_6 to form WS_2 by sulfurization. The scanning electron microscopy (SEM) images of WS_2 and WS_2/rGO hybrid nanosheets are shown in Figure 1. As-prepared WS_2 and WS_2/rGO hybrid nanosheets are shown in Figure 1 a and d, respectively. Images of freeze-dried samples are shown in Figure 1 b and e. The WS_2 nanosheets maintain their structure without any noticeable change after freeze-drying. However, the as-prepared WS_2/rGO hybrid nanosheets were found to shrink after freeze-drying, possibly due to removal of water adsorbed on rGO (Figure 1 e). The microstructure shown in Figure 1 e is very similar to rGO hydrogels formed by hydrothermal reaction and freeze-drying of GO. The rGO hydrogels consist

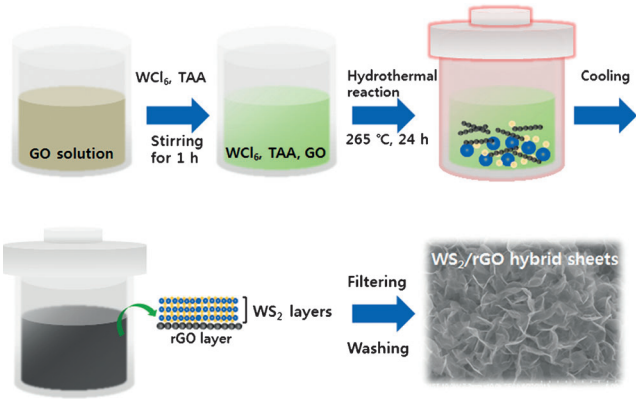

Scheme 1. Synthesis of WS_2/rGO hybrid sheets by the hydrothermal reaction.

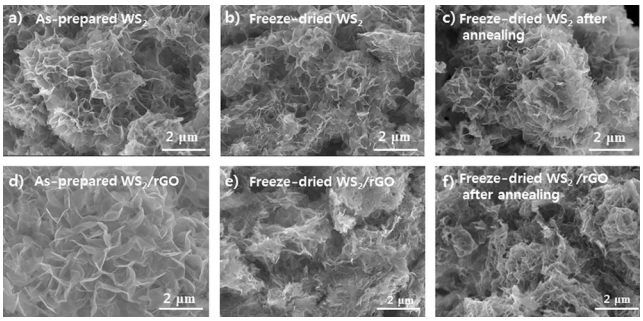

Figure 1. SEM images of a) as-prepared WS_2, b) freeze-dried WS_2, c) freeze-dried WS_2 after annealing, d) as-prepared WS_2/rGO, e) freeze-dried WS_2/rGO, and f) freeze-dried WS_2/rGO after annealing.

of flexible rGO nanosheets that are physically cross-linked.[17] Further annealing of both types of nanosheets at 300 °C did not affect the morphology of the samples as shown in Figure 1 c and f.

The WS_2 sheets on rGO were characterized by high-resolution transmission electron microscopy (HR-TEM). An image of the as-prepared WS_2/rGO hybrid sample in Figure 2 a shows overlapping nanosheets. Bilayer WS_2 nanosheets could be identified in some areas in Figure 2 a. Moire pattern and a selected-area electron diffraction (SAED) pattern from the indicated position are shown in Figure 2 b. The diffraction pattern unambiguously suggests that the WS_2 is configured in the 2H phase. Closer examination of the diffraction pattern shows two sets of hexagonal reflections from two overlapping layers, which can be attributed to

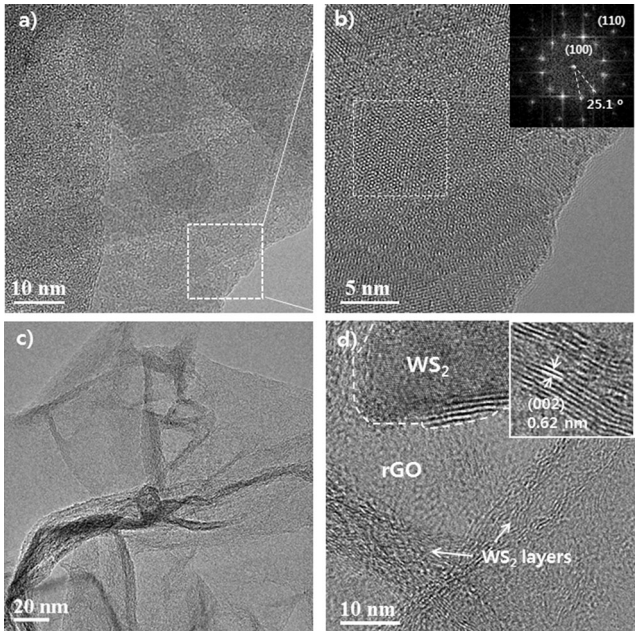

Figure 2. TEM images of WS_2/rGO hybrid nanosheets. a) As-prepared WS_2/rGO hybrid nanosheets and b) the magnified image of the marked area in (a). The inset in (b) indicates the diffraction pattern of 2H-WS_2. c) Folded edges of WS_2 sheets on rGO and d) the high-resolution image of (c). The inset shows a magnified image of some folded edges of WS_2 sheets.

a rotation angle of 25.1 degrees from the bilayers. The low- and high-magnification TEM images of WS_2/rGO hybrid sheets after annealing are shown in Figure 2c and d. The folded region in Figure 2c was selected for high-magnification observation of the edges (Figure 2d). The inset in Figure 2d clearly indicates the interlayer spacing of WS_2 is 0.62 nm, which corresponds to the *d* spacing of WS_2.[3] The WS_2 nanosheets on rGO consist of 4 to 12 layers as indicated in Figure 2d. We could not observe any edges of rGO sheets consistent with their atomically thin nature. To confirm the existence of rGO, we carried out EDAX mapping of the WS_2/rGO hybrid sheets at the location indicated in Figure 2a (see Figure S1 in the Supporting Information). Considerable carbon and oxygen elements were detected, indicating existence of rGO. We also determined the stoichiometry of WS_2 from EDAX mapping and the W:S ratio was found to be 1:2. The presence of pure WS_2 nanosheets after annealing was also confirmed by HR-TEM imaging of the hexagonal phase (see Figure S2). We have also measured the Braun–Emmet–Teller (BET) surface of the pure and hybrid nanosheets and found them to range from 10–20 $m^2 g^{-1}$). (See Figure S3) The low values of surface areas in the hybrid sheets may be attributed to intimate contacts of rGO and WS_2 sheets.

X-ray diffraction (XRD) spectra of WS_2 and WS_2/rGO hybrid nanosheets are shown in Figure 3a and Figure S4. The reflections at 14.1°, 33°, 58.2° for as-prepared WS_2 and freeze-dried WS_2 nanosheets, corresponding to (002), (100), and (110) planes, indicate the presence of the hexagonal phase.[3,5] Although some impurity peaks including those of WO_2 were observed, they disappeared after annealing.[18] The impurities may be from oxidation of WS_2. The peaks for WS_2 nanosheets after annealing appeared at 14.2°, 33.3°, and 58.4° and were sharper, suggesting improved crystallinity. The XRD pattern

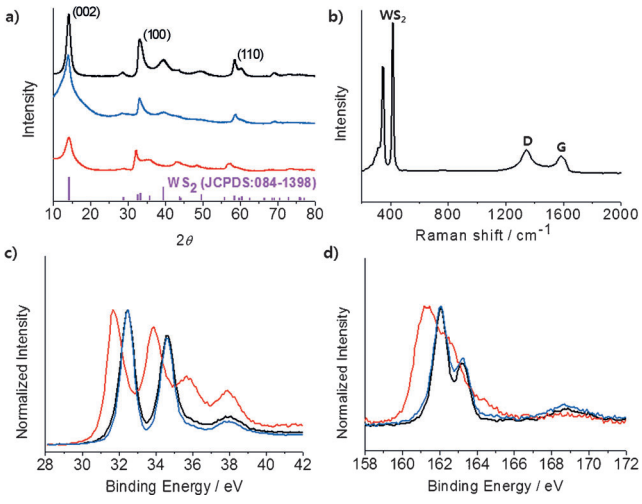

Figure 3. a) XRD patterns of freeze-dried WS_2 after annealing (black curve), freeze-dried WS2/rGO hybrid nanosheets after annealing (blue curve), and freeze-dried WS2/rGO hybrid nanosheets (red curve). b) Raman spectrum of the hybrid. XPS analysis of c) W $4f_{7/2\text{-}5/2}$ peaks and d) S $2p_{3/2\text{-}1/2}$ for the freeze-dried WS_2 nanosheets after annealing (black curve), freeze-dried WS_2/rGO hybrid nanosheets after annealing (blue curve), and freeze-dried WS2/rGO hybrid nanosheets (red curve).

is also consistent with JPCDS card number 084-1398 for pure hexagonal WS_2. Thd d-spacing of 0.62 nm, consistent with the TEM result, was calculated from the primary (002) diffraction peak. In case of as-prepared WS_2/rGO hybrid nanosheets, some impurity peaks were present along with slight shifts of peak positions and broadening. The crystallinity of WS_2 in the hybrid nanosheets also improved after annealing. However, the peaks in the hybrid samples are slightly less sharp, suggesting that the presence of rGO induces small disorder in the WS_2 structure. The (002) peak of rGO was absent from the XRD samples, consisting with lack of substantial stacking of these layers.[5,6c,19]

Our results suggest that GO acts to facilitate the growth of WS_2 nanosheets, which may be attributed to the strong interactions between the functional groups on GO and precursors. The representative Raman spectrum of WS_2/rGO hybrid nanosheets is shown in Figure 3b. Characteristic peaks for WS_2 at 350 cm^{-1} and 415 cm^{-1} corresponding to the E_{2g} and A_{1g} modes, respectively, and D and G bands of rGO can be clearly seen.[13b,20]

W $4f_{7/2\text{-}5/2}$ and S $2p_{3/2\text{-}1/2}$ binding energies obtained from X-ray photoelectron spectroscopy (XPS) are shown in Figure 3c and d. For the WS_2/rGO sheets after annealing, doublet peaks for binding energy of W $4f_{7/2\text{-}5/2}$ appeared at 32.5 and 34.6 eV, indicating an oxidation state of W^{4+} (Figure 3c), and the doublet peaks for S $2p_{1/2\text{-}3/2}$ appeared at 162.2 and163.3 eV, indicating S^{2-} (Figure 3d).[12] These peaks in the hybrid nanosheets were identical to those of pure WS_2 with high crystallinity. For the freeze-dried WS_2/rGO, the doublet peaks for the binding energy of W $4f_{7/2\text{-}5/2}$ and S $2p_{3/2\text{-}1/2}$ appear at 31.67 and 33.85 eV and at 161.4 and 162.4 eV, respectively. These peaks were broader than those of WS_2/rGO after annealing. There was a shift of about 1 eV which can be attributed to adsorption of oxygen and water molecules.[21] Furthermore, the peak at 35.7 eV was observed only in the freeze-dired WS_2/rGO sheets, which may be due to WO_2.[22]

Our analyses suggest that it is possible to fabricate high-quality WS_2 and WS_2/rGO hybrids by hydrothermal synthesis. To demonstrate their feasibility in technologically important applications, we investigated the electrocatalytic HER properties of WS_2/rGO hybrid nanosheets deposited on a glassy carbon electrode. The polarization curves (*I–V* plot) from electrodes made from freeze-dried WS_2/rGO and freeze-dried WS_2/rGO after annealing yielded overpotentials ranging from −150–−200 mV versus reversible hydrogen electrode (RHE). The overpotential of pure WS_2 nanosheets was measured to be −350 mV vs. RHE. At −300 mV, the cathode current density was 23 mA cm^{-2}, which is much higher than that observed for freeze-dried WS_2/rGO (7 mA cm^{-2}) and WS_2 (5 mA cm^{-2}). The Tafel plots derived from these data are shown in Figure 4b where the linear portions were fitted to the Tafel equation to determine the slopes. The Tafel plots reveal a slope of 140 mV dec^{-1} for annealed WS_2, 100 mV dec^{-1} for freeze-dried WS_2/rGO, and 58 mV dec^{-1} for freeze-dried WS_2/rGO after annealing. The much lower Tafel slope value for freeze-dried WS_2/rGO after annealing is due to the formation of an interconnected conducting network by the underlying rGO so that rapid electron transport from the electrode to the less-conducting WS_2 can occur.[13b]

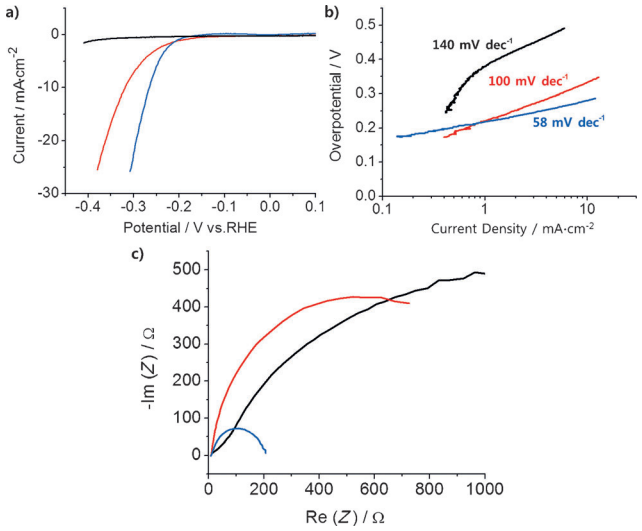

Figure 4. a) Polarization curves, b) corresponding Tafel plots recorded on glassy carbon electrodes with a catalyst loading of 400 μg cm$^{2-2}$, and c) alternating current impedance spectra of freeze-dried WS_2 nanosheets after annealing (black curve), freeze-dried WS_2/rGO hybrid nanosheets after annealing (blue curve), and freeze-dried WS2/rGO hybrid nanosheets (red curve).

HER performance of TMDs is currently limited by poor electrical transport and inefficient electrical contact between the catalyst and the electrode substrate.[23] Measurements shown in Figure 4c confirm that the impedance system is substantially lower in the WS_2/rGO nanosheets electrodes. In addition to better charge transfer, improved crystallinity of WS_2 after annealing along with the removal of oxidized impurities may improve the catalytic performace.

In conclusion, we have successfully fabricated WS_2 and WS_2/rGO hybrid nanosheets by hydrothermal synthesis. The WS_2/rGO hybrid nanosheets exhibit promising catalytic properties for HER. We attribute the better performance to the formation of an interconnected conducting rGO network that facilitates rapid electron transfer from the electrode to the catalyst and improvement of WS_2 crystallinity after annealing. Specifically the WS_2/rGO catalysts exhibit overpotential ranging from −150−−200 mV with Tafel slope of 58 mV dec^{-1}. Synthesis of WS_2 by hydrothermal method has been challenging but here we demonstrate that high-quality WS_2 nanosheets can be fabricated. Since the hydrothermal method is reasonably scalable, it may be useful for production of large quantities of TMD nanosheets for applications where large quantities are required.

Received: August 25, 2013
Revised: September 25, 2013
Published online: November 7, 2013

Keywords: electrocatalysis · hybrid materials · hydrogen · reduced graphene oxide · tungsten disulfide

[1] a) M. Chhowalla, H. S. Shin, G. Eda, L.-J. Li, K. P. Loh, H. Zhang, *Nat. Chem.* **2013**, *5*, 263–275; b) Q. H. Wang, K. Kalantar-Zadeh, A. Kis, J. N. Coleman, M. S. Strano, *Nat. Nanotechnol.* **2012**, *7*, 699–712.
[2] a) C. J. Carmalt, I. P. Parkin, E. S. Peters, *Polyhedron* **2003**, *22*, 1499–1505; b) J. N. Coleman, M. Lotya, A. O'Neill, S. D. Bergin, P. J. King, U. Khan, K. Young, A. Gaucher, S. De, R. J. Smith, *Science* **2011**, *331*, 568–571.
[3] J.-W. Seo, Y.-W. Jun, S.-W. Park, H. Nah, T. Moon, B. Park, J.-G. Kim, Y. J. Kim, J. Cheon, *Angew. Chem.* **2007**, *119*, 8984–8987; *Angew. Chem. Int. Ed.* **2007**, *46*, 8828–8831.
[4] Z. Wu, B. Fang, A. Bonakdarpour, A. Sun, D. P. Wilkinson, D. Wang, *Appl. Catal. B* **2012**, *125*, 59–66.
[5] K. Shiva, H. S. S. Ramakrishna Matte, H. B. Rajendra, A. J. Bhattacharyya, C. N. R. Rao, *Nano Energy* **2013**, DOI: 10.1016/j.nanoen.2013.02.001.
[6] a) H. Li, W. Li, L. Ma, W. Chen, J. Wang, *J. Alloys Compd.* **2009**, *471*, 442–447; b) S. Wang, G. Li, G. Du, X. Jiang, C. Feng, Z. Guo, S.-J. Kim, *Chin. J. Chem. Eng.* **2010**, *18*, 910–913; c) K. Chang, W. Chen, *ACS Nano* **2011**, *5*, 4720–4728.
[7] Y. Shang, J. Xia, Z. Zu, W. Chen, *J. Dispersion Sci. Technol.* **2005**, *26*, 635–639.
[8] H. A. Therese, J. Li, U. Kolb, W. Tremel, *Solid State Sci.* **2005**, *7*, 67–72.
[9] B. Gao, H. Fan, X. Zhang, *J. Phys. Chem. Solids* **2012**, *73*, 423–429.
[10] D. Chen, M. Liu, L. Yin, T. Li, Z. Yang, X. Li, B. Fan, H. Wang, R. Zhang, Z. Li, H. Xu, H. Lu, D. Yang, J. Sun, L. Gao, *J. Mater. Chem.* **2011**, *21*, 9332–9342.
[11] T. F. Jaramillo, K. P. Jørgensen, J. Bonde, J. H. Nielsen, S. Horch, I. Chorkendorff, *Science* **2007**, *317*, 100–102.
[12] Y.-H. C. T.-Y. Chen, C.-L. Hsu, K.-H. Wei, C.-Y. Chiang, L.-J. Li, *Int. J. Hydrogen Energy* **2013**, DOI: 10.1016/j.ijhydene.2013.07.021.
[13] a) J. Kibsgaard, Z. Chen, B. N. Reinecke, T. F. Jaramillo, *Nat. Mater.* **2012**, *11*, 963–969; b) Y. Li, H. Wang, L. Xie, Y. Liang, G. Hong, H. Dai, *J. Am. Chem. Soc.* **2011**, *133*, 7296–7299.
[14] D. Voiry, H. Yamaguchi, J. Li, R. Silva, D. C. B. Alves, T. Fujita, M. Chen, T. Asefa, V. B. Shenoy, G. Eda, M. Chhowalla, *Nat. Mater.* **2013**, *12*, 850–855.
[15] A. Margolin, F. Deepak, R. Popovitz-Biro, M. Bar-Sadan, Y. Feldman, R. Tenne, *Nanotechnology* **2008**, *19*, 095601.
[16] X. L. Li, J. P. Ge, Y. D. Li, *Chem. Eur. J.* **2004**, *10*, 6163–6171.
[17] a) Y. Xu, Z. Lin, X. Huang, Y. Liu, Y. Huang, X. Duan, *ACS Nano* **2013**, *7*, 4042–4049; b) Y. Xu, K. Sheng, C. Li, G. Shi, *ACS Nano* **2010**, *4*, 4324–4330.
[18] a) C. Feng, L. Huang, Z. Guo, H. Liu, *Electrochem. Commun.* **2007**, *9*, 119–122; b) S. Jeon, K. Yong, *J. Mater. Chem.* **2010**, *20*, 10146–10151.
[19] C. S. Rout, B.-H. Kim, X. Xu, J. Yang, H. Y. Jeong, D. Odkhuu, N. Park, J. Cho, H. S. Shin, *J. Am. Chem. Soc.* **2013**, *135*, 8720–8725.
[20] H. S. S. Ramakrishna Matte, A. Gomathi, A. K. Manna, D. J. Late, R. Datta, S. K. Pati, C. N. R. Rao, *Angew. Chem.* **2010**, *122*, 4153–4156; *Angew. Chem. Int. Ed.* **2010**, *49*, 4059–4062.
[21] I. Martin, P. Vinatier, A. Levasseur, J. C. Dupin, D. Gonbeau, *J. Power Sources* **1999**, *81–82*, 306–311.
[22] A. Benadda, A. Katrib, J. W. Sobczak, A. Barama, *Appl. Catal. A* **2004**, *260*, 175–183.
[23] M. A. Lukowski, A. S. Daniel, F. Meng, A. Forticaux, L. Li, S. Jin, *J. Am. Chem. Soc.* **2013**, *135*, 10274–10277.